J. Electrochem. Sci. Eng. **15(1)** (2024) 2438; http://dx.doi.org/10.5599/jese.2438

Open Access : : ISSN 1847-9286
www.jESE-online.org

Original scientific paper

Polyaniline prepared by Fe_3O_4 catalysed eco-friendly synthesis as electrocatalyst for efficient water electrolysis

Jadranka Milikić[1], Jana Mišurović[1,2], Lazar Rakočević[3], Igor A. Pašti[1], Gordana Ćirić-Marjanović[1] and Biljana Šljukić[1,✉]

[1]*University of Belgrade - Faculty of Physical Chemistry, Studentski trg 12-16, 11158, Belgrade, Serbia*
[2]*Now at University of Montenegro, Faculty of Metallurgy and Technology, Cetinjski put, bb, 81000 Podgorica, Montenegro*
[3]*University of Belgrade, "VINČA" Institute of Nuclear Sciences, National Institute of the Republic of Serbia, Mike Petrovića Alasa 12-14, 11000, Belgrade, Serbia*

Corresponding authors: ✉biljka@ffh.bg.ac.rs

Received: July 22, 2024; Accepted: September 9, 2024; Published: October 30, 2024

Abstract

Preparing cost-effective and highly active catalysts for electrocatalytic hydrogen evolution reaction is crucial for developing hydrogen-based technologies. Hence, four conductive polyanilines, prepared by the environmentally-friendly approach using Fe_3O_4 nanoparticles/H_2O_2 as the catalyst/main oxidant system (PANI/Fe_3O_4), were investigated for the first time as electrocatalysts for hydrogen evolution reaction (HER) in acidic media (0.1 M H_2SO_4) by using voltammetry and chronoamperometry. PANI/Fe_3O_4 electrodes exhibited Tafel slope values in the -171 to -246 mV dec^{-1} range depending on the synthesis conditions – Fe_3O_4/aniline mass ratio and polymerization time. The sample PANI/Fe_3O_4-II(3) prepared with shorter reaction time and higher Fe_3O_4/aniline mass ratio showed the best electrocatalytic behaviour reflected in the lowest onset potential (-0.286 V), the lowest overpotential to reach a current density of -10 mA cm^{-2}, the highest current density, the lowest HER activation energy (10 kJ mol^{-1}), and the lowest charge-transfer resistance (5.3 Ω) under HER conditions. Materials were characterized by scanning electron microscopy with energy dispersive X-ray spectroscopy, X-ray photoelectron spectroscopy and electrochemical impedance spectroscopy, and differences in their electrocatalytic HER performance were explained by differences in their content of Fe_3O_4, surface and electrical properties. Moreover, the possibility of using PANI/Fe_3O_4-II(3) as HER electrocatalyst in a wider range of pH (i.e. in alkaline media as well) and as a bifunctional electrocatalyst, i.e. for oxygen evolution reaction beside HER, was also examined.

Keywords

Hydrogen evolution reaction; oxygen evolution reaction; conducting polymers; transition metal oxides; electrocatalysis

Introduction

Intensive research in electrochemistry is devoted to finding the appropriate way to transform and store hydrogen energy [1-5]. The electrochemical hydrogen evolution reaction (HER) is probably the most important reaction to produce hydrogen (H_2) in a simple, clean, and efficient way. HER mechanism in acidic media takes two possible pathways: Volmer-Heyrovsky (Eqs. 1 and 2) or Volmer-Tafel pathway (Eqs. 1 and 3) [6]:

$H_3O^+ + e^- + * \rightarrow H_{ads} + H_2O$ Volmer reaction (1)

$H_3O^+ + e^- + H_{ads} \rightarrow H_2 + H_2O + *$ Heyrovsky reaction (2)

$H_{ads} + H_{ads} \rightarrow H_2 + *$ Tafel reaction (3)

where * represents an active site on the surface of the electrocatalyst.

Many electrocatalysts have been tested for HER, where platinum (Pt) is the most active, demonstrating fast HER kinetics with low overpotential and high current densities [5]. Still, the application of this metal on an industrial scale is limited because of its high price. Finding an appropriate electrocatalyst for HER that is inexpensive and efficient, with good performance and stability during HER, is vital for future applications in the industry and energy systems. Electrocatalysts based on nonprecious metals such as iron (Fe), nickel (Ni), cobalt (Co), and copper (Cu) are investigated for HER in both acidic and alkaline solutions [7-11]. Composites of MoCoFeS (MCFS) with different amounts of reduced graphene oxide (rGO), MCFS/rGO, were examined for HER in acidic media (0.5 M H_2SO_4) [10]. It was shown that MCFS/rGO electrocatalysts with a mass ratio of rGO up to 0.4 have good HER activity with high current densities and low Tafel slopes of *ca.* 50 to 60 mV dec^{-1} [10]. Fe, Co, and Fe-Co alloy encapsulated in nitrogen-doped carbon nanotubes (CNTs) were characterised for HER by voltammetry and density functional theory (DFT) calculations in acidic media [6]. HER activity of these electrocatalysts significantly increased with increasing the amount of nitrogen. Fe-Co alloy showed the best performance for HER with the smallest overpotential and the onset potential value of *ca.* 70 mV *vs.* RHE in 0.1 M H_2SO_4 [6]. Iron phosphide (FeP) nanoparticles synthesised by phosphorization of α-Fe_2O_3 showed excellent HER performance and stability in 0.5 M H_2SO_4 due to the change of surface-charge-transfer resistance [12]. $Fe_{1.89}Mo_{4.11}O_7/MoO_2$ showed good stability during HER in both acidic and alkaline media [13]. The Tafel slope and an exchange current density were calculated to be -47 and 0.072 mA cm^{-2}, respectively, in acidic media [13]. A hybrid composite consisting of Fe_3C nanorods encapsulated in N-doped carbon nanotubes (CNTs) was presented as a good HER electrocatalyst in both alkaline and acidic media with Tafel slope of -113 and -97 mV dec^{-1} in these media, respectively [14]. Fe_3O_4 on graphite sheets were synthesized by one-pot hydrothermal method and exhibited favourable HER kinetics in alkaline media with low Tafel slope of -78 mV dec^{-1}, as well as long-term stability under HER conditions [15].

Conductive polymers have broad applications in electrochemical energy conversion and storage [16]. Polyaniline (PANI), as a low-cost conductive polymer, has excellent chemical and physical properties and a delocalized π-conjugated structure [17,18]. It can be easily synthesized [18-20] and combined with other active materials, improving the electrocatalytic activity, conductivity, and stability [17,21,22]. PANI was shown to be a useful electrode material for promoting HER [23-26] and oxygen evolution reaction (OER) [27-31] over a wide pH range. It is frequently used as metal electrocatalyst support due to its advantages, such as good flexibility, variety of controllable morphologies, and ability to provide more active sites [32,33]. It was also reported that the conductive PANI is favourable for HER due to its sufficient protonated sites [33]. For instance, several electrocatalysts combining PANI polymer and semiconductor $Na_4Ge_9O_{20}$ as a support for low amounts of Pt nano-

particles (Pt NPs) were investigated for HER in 0.5 M H_2SO_4 [17]. 5 wt.% Pt/$Na_4Ge_9O_{20}$-PANI gave an overpotential of -33 mV, *i.e.,* close to that of commercial 20 wt.% Pt/C electrocatalyst (21 mV), demonstrating that PANI and Pt NPs improve HER kinetics due to the increased number of transferring electrons and active sites [17]. RuO_2-Ta_2O_5/PANI composite presented the HER catalytic process by Volmer-Heyrovsky mechanism where Tafel slope was found to be -69.2 mV dec^{-1} and the overpotential amounted to -185 mV in 0.5 M H_2SO_4 [34]. Nevertheless, the electrocatalysis of HER using PANI-based materials with low concentrations of non-noble metals was not addressed in detail, and such studies could pave the way toward the development of low-cost electrocatalysts for acidic water electrolysis as non-noble metals (Fe, Co, Ni) are generally unstable in acidic media.

The common method for synthesizing PANI is the chemical oxidative polymerization of aniline, most frequently using the powerful oxidant ammonium peroxydisulfate (APS) [18]. This type of reaction also gives undesired inorganic by-products (*e.g.* ammonium hydrogen sulphate) that should be removed by the post-synthetic treatments. For the most environmentally friendly polymerization of aniline, the best oxidizing agent would be hydrogen peroxide (H_2O_2) since the product of its reduction is water. However, due to the low reactivity of H_2O_2, its usage for efficient aniline polymerization leading to PANI of high electrical conductivity needs the addition of a suitable catalyst. Different catalysts were explored for this purpose, such as transition metal salts [35] and peroxidase-type enzymes [20,36].

In this study, four PANI/Fe_3O_4 materials were synthesized under different reaction conditions via environmentally friendly aniline oxidative polymerization by using H_2O_2 as a main oxidant, Fe_3O_4 NPs as a catalyst, and a very small amount of ammonium peroxydisulfate (APS) [37] were examined as electrocatalysts for HER in acidic media (0.1 M H_2SO_4) by voltammetry and chronoamperometry. The surface and electrical properties of materials, determined by scanning electron microscopy with energy dispersive X-ray analysis (SEM-EDX), X-ray photoelectron spectroscopy (XPS), and electrochemical impedance spectroscopy (EIS), were correlated with their electrocatalytic performance. The possibility of using PANI/Fe_3O_4 as HER electrocatalyst in a wider pH range and as a bifunctional electrocatalyst, *i.e.,* for OER beside HER, was also examined.

Experimental

PANI/Fe_3O_4 materials were prepared by the oxidative chemical polymerization of aniline monomer (monomer solution containing 0.2 M aniline hydrochloride, formed *in situ*, and 0.2 M HCl obtained by mixing specified amounts of aniline (1.824 ml) and HCl (3.357 ml) in water (100 ml) with eco-friendly oxidant H_2O_2 (0.25 M) and a small amount of APS (0.1 mM), in the presence of catalytic amounts of Fe_3O_4 NPs, by the procedures reported in [37]. Fe_3O_4 NPs were synthesized by the procedure described in [37], starting from the aqueous solution of ferric chloride hexahydrate and ferrous sulphate heptahydrate and performing precipitation of Fe_3O_4 NPs by NH_4OH. H_2O_2 was successfully used as the main oxidant thanks to Fe_3O_4 NPs, which served as a catalyst, while a small amount of added APS enabled efficient initiation [37]. All PANI/Fe_3O_4 samples were prepared at mole ratios [H_2O_2]/[aniline] = 1.25 and [APS]/[aniline] = 0.0005. Samples synthesized at mass ratio Fe_3O_4 NPs/aniline of 0.0015 were denoted PANI/Fe_3O_4-I(3) and PANI/Fe_3O_4-I(7), and the samples synthesized at mass ratio Fe_3O_4 NPs/aniline of 0.015 were denoted PANI/Fe_3O_4-II(3) and PANI/Fe_3O_4-II(7), where the labels (3) and (7) refer to polymerization times of 3 days and 7 days, respectively.

LCR meter, model LCR-6100 (GW Instek, Taiwan) at room temperature and constant frequency (1.0 kHz) on a pellet pressed between two stainless steel pistons (under pressure of ~4 MPa by a manual hydraulic press) was used for measuring the electrical conductivity of powdered samples [37].

The morphology of the samples and their elemental composition were characterized by SEM-EDX using a scanning electron microscope JEOL JSM-660LV, along with elemental mapping. Prior to the analysis, samples were coated with a thin layer of gold using LEICA SCD005 Sputter Coater.

XPS analysis was performed using SPECS Systems with XP50M X-ray source for Focus 500 X-ray monochromator and PHOIBOS 100/150 analyser using AlKα (1486.74 eV) anode at a 12.5 kV and 32 mA as a source. Survey spectra (1000 - 0 eV binding energy) were recorded with a constant pass energy of 40 eV, step size 0.5 eV, and dwell time of 0.2 s in the FAT mode. Detailed spectra of C 1s, N 1s, and O 1s were recorded with a constant pass energy of 20 eV, step size of 0.1 eV, and dwell time of 2s in the FAT mode.

The catalytic inks were prepared by ultrasonically dispersing powder mixtures of each of the four samples (4 mg) and commercial Vulcan XC72 conductive carbon black (1 mg) in 2 wt.% polyvinylidene fluoride solution in N-methyl-2-pyrrolidone (125 µl). 10 µL of each ink was deposited onto a glassy carbon tip and dried at 110 °C overnight.

Electrochemical measurements were performed using PAR 273A Princeton Potentiostat/Galvanostat in a one-compartment glass cell of 50 ml volume. Pt wire or graphite rod served as a counter electrode, and saturated calomel electrode (SCE) served as a reference electrode. All potentials within this paper were converted to the reversible hydrogen electrode (RHE) scale. 0.1 M H_2SO_4 solution was used as an electrolyte.

HER polarization curves were recorded at 2 mV s^{-1} and different temperatures from 25 to 75 °C using a Haake F3 bath. Chronoamperometric (CA) curves of all PANI/Fe_3O_4 electrocatalysts were recorded at a potential 0.1 V more negative than the onset potential for 1 h.

Cyclic voltammetry (CV) measurements of four PANI/Fe_3O_4 electrocatalysts were performed in 0.1 M H_2SO_4 saturated with nitrogen at different scan rates ranging from 10 to 300 mV s^{-1}. Electrochemical impedance spectroscopy (EIS) measurements were conducted in the frequency range from 100 kHz to 0.1 Hz, with 5 mV amplitude, at different potentials.

HER polarization curves were also recorded in 8 M KOH as an electrolyte, with this concentration corresponding to the KOH concentration used in industrial alkaline water electrolysers. Finally, polarization curves were recorded under oxygen evolution reaction conditions at 10 mV s^{-1} in both 0.1 M H_2SO_4 and 8 M KOH.

Results and discussion

Electrical conductivity and morphology of PANI/Fe_3O_4 electrocatalysts

A detailed characterization of PANI/Fe_3O_4 samples showed that the products obtained were PANIs in their conductive form, emeraldine salt (ES) [37]. This finding, together with the presence of Fe_3O_4 NPs in all samples (although in very small, catalytic amounts), makes these materials promising candidates for HER. Samples PANI/Fe_3O_4-II(3) and PANI/Fe_3O_4-II(7), synthesized at a higher mass ratio of Fe_3O_4 NPs/aniline (0.015), exhibited good electrical conductivities of 10 and 15 mS cm^{-1}, respectively. Conversely, the other two samples, PANI/Fe_3O_4-I(3) and PANI/Fe_3O_4-I(7), which were prepared at lower mass ratio Fe_3O_4 NPs/ aniline (0.0015), showed lower conductivities of 4.6 and 7.3 mS cm^{-1}, respectively [37]. SEM images reveal mutually similar morphology of PANI/Fe_3O_4 samples, which is predominantly granular, with irregularly shaped particles (Figure 1A, 1C, 1E, 1G).

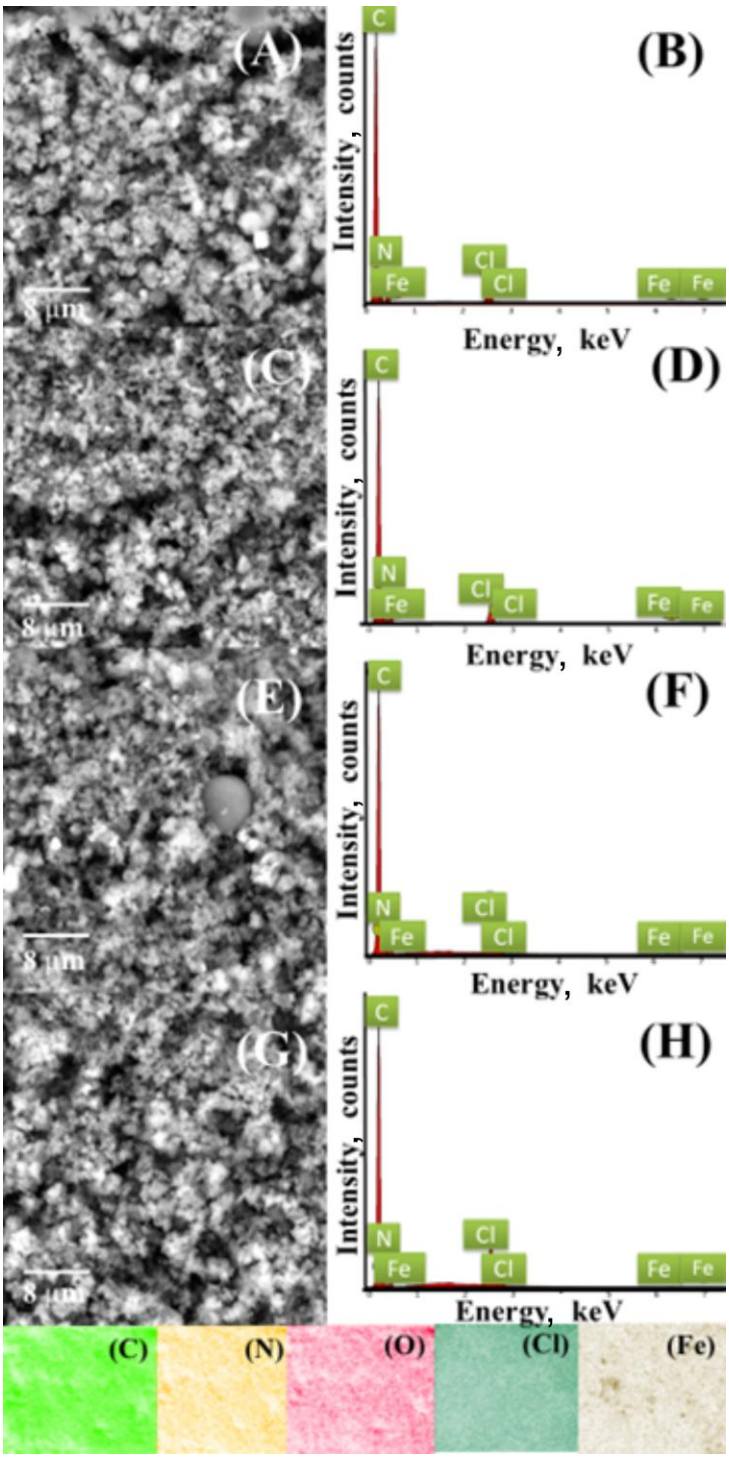

Figure 1. *A, C, E, G: SEM images of four PANI/Fe_3O_4 electrocatalysts. B, D, F, H: their corresponding EDX spectra with elemental mapping of PANI/Fe_3O_4-I(3)*

EDX analysis (Figure 1B, 1D, 1F, 1H) confirmed the presence of C, N, Fe, O, and Cl, with their distribution evidenced by elemental mapping. The presence of chlorine could be expected since the monomer solution contained aniline hydrochloride and HCl in excess so that Cl^- ions are incorporated in the final PANI/Fe_3O_4 mainly as dopant anions in PANI-ES conducting form. The presence of chlorine covalently bound to aromatic rings (C-Cl) is also possible [38]. The presence of Fe revealed by EDX in the samples follows previous XRD analysis where diffractograms of PANI/Fe_3O_4 samples showed peaks characteristic for the crystalline magnetite and confirmed incorporation of Fe_3O_4 NPs in the PANI matrix during synthesis [37]. Fe amount was determined by EDX mapping to be 0.64, 0.46, 0.35 and 0.25 wt.% for II(3), I(3), II(7), and I(7) samples, respectively, revealing that

longer polymerization time led to decrease in Fe content, as might be expected due to increased yield of PANI.

XPS survey spectra for PANI/Fe_3O_4 samples are shown in Figure 2A**.** They confirm the presence of C, N, O, and Cl in all four samples by their characteristic peaks. Peaks of Fe are not visible in any of the spectra. The most likely reason is that a thin layer of PANI covers Fe (from Fe_3O_4 NPs used in catalytic amounts). Therefore, as a strictly surface analysis, XPS could not detect Fe. All four samples show similar survey spectra that originate from PANI. The atomic percentages of 80.3, 10.8, 5.3, and 3.6 % were obtained for C, N, O, and Cl elements, respectively, derived from survey XPS spectra for the PANI/Fe_3O_4-II (3) sample. The peak at *ca.* 200 eV corresponds to Cl 2p, where chlorine can exist in the form of ionic (Cl^-) or covalent (C-Cl) species whose peak positions are close, *ca.* 198 and 200 eV, respectively, similar to what was reported for PANI-ES doped with HCl [39].

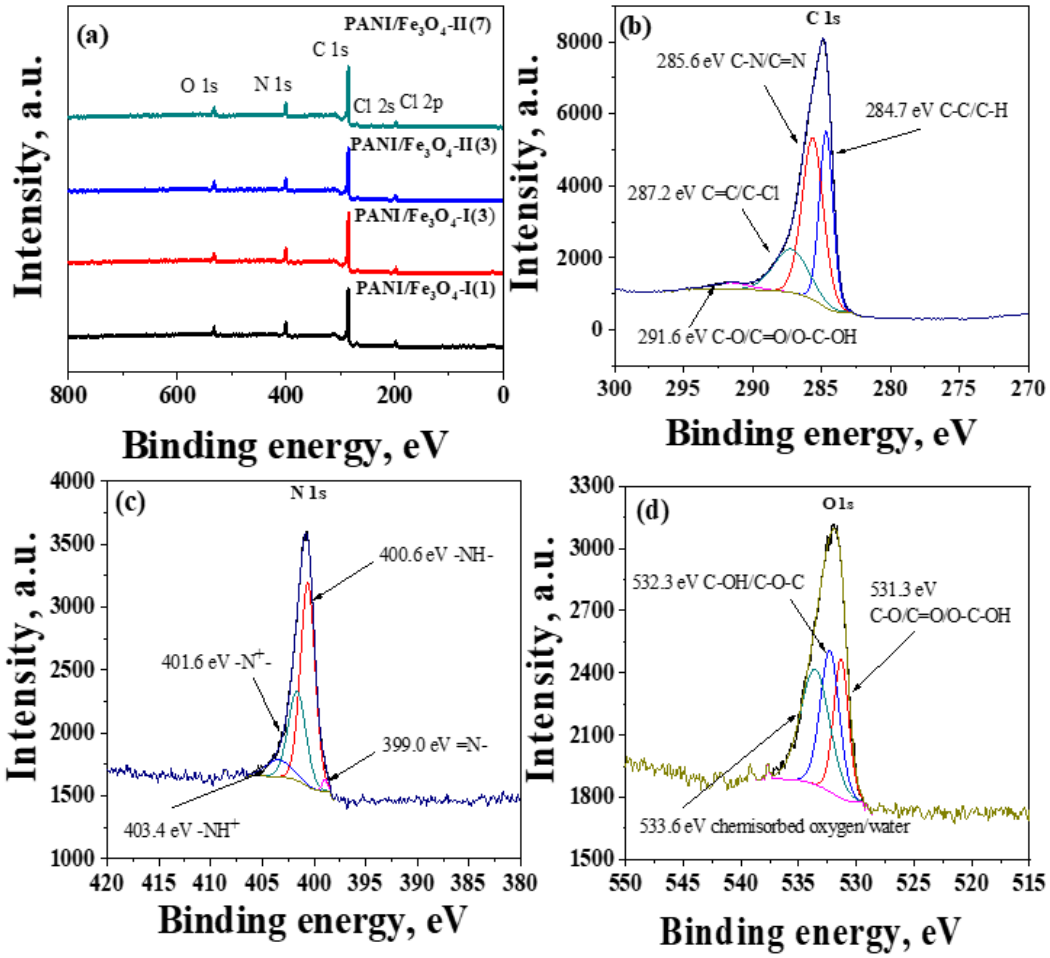

Figure 2. *A: XPS survey spectra for all PANI/Fe_3O_4 samples; B: Detailed XPS spectra of C 1s; C: Detailed XPS spectra of N 1s; D: detailed XPS spectra of O 1s*

Detailed XPS C 1s signal for sample PANI/Fe_3O_4-II(3), which showed the highest electrocatalytic activity (see below), is shown in Figure 2B. Carbon peak can be deconvoluted into four components. The small intensity component at 291.6 eV originates from carbon-oxygen bonds in C-O, C=O, or O-C-OH groups at similar binding energies. The component at 287.2 eV corresponds to either a double C=C bond or a carbon bound to chlorine (C-Cl) located at similar binding energies. The third component at 285.6 eV originates from bonds of carbon and nitrogen in polaron and bipolaron PANI structures, C-N^+ and C=N^+. The last component at 284.8 eV corresponds to either C-C or C-H bond in the PANI backbone structure [40-43].

High-resolution N 1s spectrum for sample PANI/Fe_3O_4-II(3) is shown in Figure 2C. Spectra can be deconvoluted into four components. Components at 403.4, 401.6, 400.6 and 399.0 eV can be attributed to positively charged N species -NH^+ and -N^+-, benzenoid amine -NH- and quinonoid imine =N- functional groups, respectively. These functional groups correspond to the PANI structure confirming the nature of the surface of samples [39].

Detailed XPS spectra of O 1s for sample PANI/Fe_3O_4-II(3) (Figure 2D) can be deconvoluted into three components. The component at 533.6 eV is attributed to oxygen originating from chemisorbed water on the surface of PANI. The component at 532.3 eV is attributed to different carbon-oxygen C-OH or C-O-C bonds, and a component at 531.3 eV that is also assigned to either C-O, C=O or O-C-OH bonds [39], where C=O (for example, present in benzoquinone species) can be formed by partial hydrolysis of reaction intermediates during PANI synthesis [18].

All the detailed spectra confirm that the surface of the samples consists of a layer of PANI polymer that covers the entire surface and is overlayed over any present Fe.

Percentages for each functional group present in high-resolution XPS spectra of C 1s, N 1s and O 1s for PANI/Fe_3O_4-II(3) are summarized in Table 1.

Table 1. *Content of individual functional groups for PANI/Fe_3O_4-II(3) derived from detailed XPS spectra*

C 1s	C-C/C-H	C-N/C=N	C=C/C-Cl	C-O/C=O/C-OH
Content, %	31.5	45.4	19.8	3.3
N 1s	=N-	-NH-	-N^+-	-NH^+
Content, %	59.0	30.8	8.9	1.3
O 1s	C-O/C=O/O-C-OH	C-O-C/C-OH	Chemisorbed water	
Content, %	25.7	33.1	41.2	

Investigation of HER and OER at PANI/Fe_3O_4 electrocatalysts

The HER onset potentials in 0.1 M H_2SO_4, defined as the potential to reach a current density of -1 mA cm^{-2} [44], increased in the order PANI/Fe_3O_4-II(3) (-0.286 V) < PANI/Fe_3O_4-II(7) (-0.397 V) < < PANI/Fe_3O_4-I(7) (-0.564 V) < PANI/Fe_3O_4-I (3) (-0.598 V), (Figure 3A). The highest current densities are obtained for PANI/Fe_3O_4-II(3), followed by PANI/Fe_3O_4-II(7), PANI/Fe_3O_4-I(7) and PANI/Fe_3O_4-I(3). The HER overpotential at the current density of -10 mA cm^{-2} (η_{10}) for PANI/Fe_3O_4-II(3) is found to be -444 mV (current density of -10 mA cm^{-2} was not reached using the other three studied materials). This overpotential was determined as a difference between the potential to reach -10 mA cm^{-2} and the equilibrium potential value of the hydrogen electrode (*i.e.* referred to 0 V *vs.* RHE).

Tafel slope (b) and the exchange current density (j_0) values for HER at four studied materials were calculated to estimate HER kinetics and their values are presented in Table 2. Tafel slope values increased in the order PANI/Fe_3O_4-II(7) (-171 mV dec^{-1}) < PANI/Fe_3O_4-II(3) (-182 mV dec^{-1}) < < PANI/Fe_3O_4-I(7) (-204 mV dec^{-1}) < PANI/Fe_3O_4-I(3) (-246 mV dec^{-1}). The Tafel slopes higher than the theoretically expected values might originate in the uncompensated resistance along with the limited number of active sites of PANI/Fe_3O_4 electrocatalysts where protons could be adsorbed. Namely, Tafel slope takes value of 30, 40 or 120 mV dec^{-1} for Tafel, Heyrovsky or Volmer step, respectively, being the rate determining step. The observed resistance might arise from the wiring, solution and substrate, as well as from a slow charge transport [45] and it is further examined by EIS (page 9, last paragraph). PANI/Fe_3O_4-II(3) gave the highest exchange current density (37 μA cm^{-2}) followed by PANI/Fe_3O_4-I(7), PANI/Fe_3O_4-I(3) and PANI/Fe_3O_4-II(7) electrocatalysts.

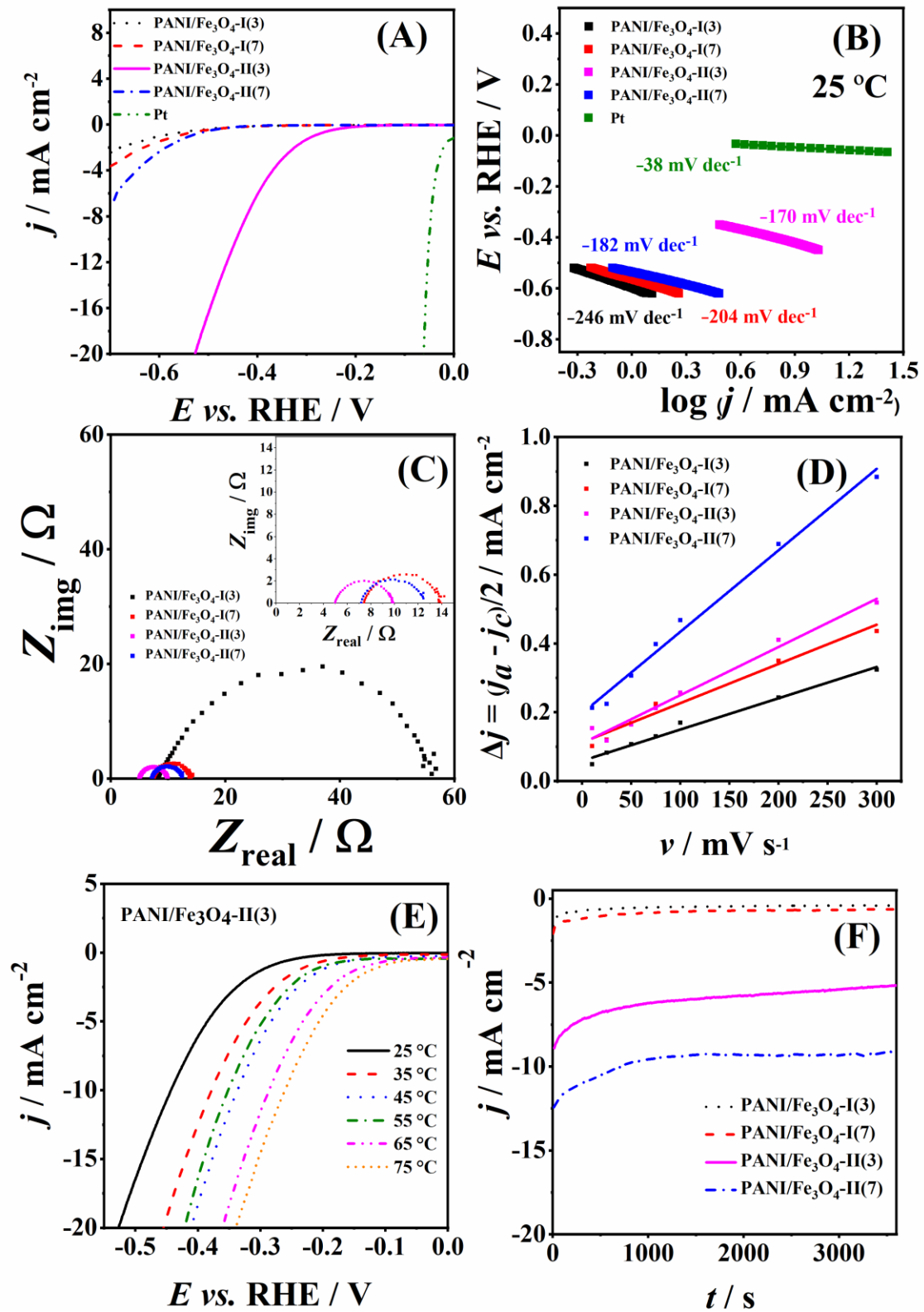

Figure 3. *A: polarization curves of four PANI/Fe_3O_4 electrocatalysts at 2 mV s^{-1} and 25 °C (IR-corrected); B: their corresponding Tafel plots; C: their Nyquist plots at -0.5 V; D: their Δj = ((j_a - j_c)/2) as a function of polarisation rate; E: polarization curves of PANI/Fe_3O_4-II(3) at temperatures from 25 to 75 °C at 2 mV s^{-1} (IR-corrected); F: chronoamperometric curves of four PANI/Fe_3O_4 electrocatalysts. All measurements were done in 0.1 M H_2SO_4 (N_2-saturated electrolyte in the case of D)*

PANI/Fe_3O_4-II(3) showed the best performance for HER in terms of the lowest onset potential, the highest current densities, the lowest value of η_{10}, and the highest exchange current density, followed by PANI/Fe_3O_4-II(7). On the other hand, PANI/Fe_3O_4-I(3) and PANI/Fe_3O_4-I(7) showed high

HER onset potential, low current densities, and low exchange current densities (Table 2), thus exhibiting poor HER activity. Some of the possible reasons for this difference in the four electrocatalysts' activity for HER are the differences in their electrical conductivities and charge transfer kinetics [46], along with differences in their hydrogen and reaction intermediates adsorption energy [47] and bonding [48]. PANI/Fe_3O_4-II(3) and PANI/Fe_3O_4-II(7) have one order of magnitude higher electrical conductivities compared to those of PANI/Fe_3O_4-I(3) and PANI/Fe_3O_4-I(7). Still, polycrystalline Pt as a benchmark HER electrocatalyst showed significantly better HER kinetic parameters compared with the presented PANI/Fe_3O_4 electrocatalysts in acidic media (Table 2). On the other hand, Pt has a much higher price than PANI/Fe_3O_4 electrodes.

Table 2. *Comparison of HER performance of PANI/Fe_3O_4 with other non-noble metal-based electrocatalysts in acidic media*

Electrocatalyst	Electrolyte	b / mV dec^{-1}	j_0 / μA cm^{-2}	Reference
PANI/Fe_3O_4-I(3)	0.1 M H_2SO_4	-246	3.6	This work
PANI/Fe_3O_4-I(7)	0.1 M H_2SO_4	-204	1.7	This work
PANI/Fe_3O_4-II(3)	0.1 M H_2SO_4	-182	37.0	This work
PANI/Fe_3O_4-II(7)	0.1 M H_2SO_4	-170	0.72	This work
Pt	0.5 M H_2SO_4	-38	460	This work
MCFS/rGO1/GC[c]	0.5 M H_2SO_4	-202.6	/	[10]
$Fe_{1.89}Mo_{4.11}O_7/MoO_2$	0.5 M H_2SO_4	-47	72.0	[13]
Fe/MoO_2	0.5 M H_2SO_4	-128	/	[13]
Fe_3C@NCNT	0.5 M H_2SO_4	-97	/	[14]
RuNi-NSs@PANI[g]	0.5 M H_2SO_4	-73.1	-	[22]
PANI/CoNiPeNF[h]	0.5 M H_2SO_4	-80	-	[47]
β-INS nanosheets[a]	0.5 M H_2SO_4	-48	14.0	[49]
Fe_2N/rGO	0.5 M H_2SO_4	-161	370.0	[50]
$Fe_{4.5}Ni_{4.5}S_8$[b]	0.5 M H_2SO_4	-72	/	[51]
NHPBA[d]	0.5 M H_2SO_4	-157	/	[52]
Fe-WOxP[e]	0.5 M H_2SO_4	-80	156.0	[53]
FeP (1:1)[f]	0.5 M H_2SO_4	-82	/	[54]
FeP (1:4)[f]	0.5 M H_2SO_4	-69	/	[54]
Ni-PANI	0.5 M H_2SO_4	-131 to -147	0.119 to 0.239	[55]

[a]iron-nickel sulfide (INS); [b]a direct 'rock' electrode; [c]MoCoFeS supported reduced graphene oxide deposited on glassy carbon (MCFS/rGO/GC; [d]nickel hydroxide array with K_3[FeIII(CN)$_6$] (NHPBA); [e]iron-doped tungsten oxide nanoplate/reduced graphene oxide nanocomposite (Fe-WOxP); [f]iron phosphide pristine; [g]Ru-doped $Ni(OH)_2$ nanosheets; [h]Nickel foam

A higher electrical conductivity, *i.e.,* lower charge-transfer resistance of PANI/Fe_3O_4-II(3) and PANI/Fe_3O_4-II(7), was confirmed by EIS measurements in 0.1 M H_2SO_4, Figure 3C. The electrolyte resistance (R_s) as the first point of Nyquist plots of PANI/Fe_3O_4-II(3), PANI/Fe_3O_4-II(7), PANI/Fe_3O_4-I(7), and PANI/Fe_3O_4-I(3) is found to be similar, *i.e.,* 5.1, 7.2, 7.5, and 8.3 Ω, respectively, indicating well-maintained geometry of the experimental setup. The charge-transfer resistance (R_{ct}) was determined to be 4.8, 5.3, and 6.3 Ω for PANI/Fe_3O_4-II(3), PANI/Fe_3O_4-II(7) and PANI/Fe_3O_4-I(7), respectively. A much higher R_{ct} value of 47.8 Ω was determined for PANI/Fe_3O_4-I(3). It can be seen that PANI/Fe_3O_4-II(3) showed very low R_{ct} steaming from the presence of the highest amount of Fe (determined by EDX mapping) and the strong electronic coupling of PANI with Fe_3O_4 [46]. Moreover, it was suggested that the interaction between PANI and Fe_3O_4 lowers the contact resistance and further impacts HER adsorption/desorption of reaction intermediates. This assumption is consistent with highest content of Fe in PANI/Fe_3O_4-II(3) measured by EDX, as well as with higher content of Fe_3O_4 NPs revealed by XRD measurements [37] in PANI/Fe_3O_4-II(3) (mass ratio Fe_3O_4/aniline = 0.015) than in PANI/Fe_3O_4-I(3) (mass

ratio Fe_3O_4/aniline = 0.0015), both samples synthesized with the same polymerization time. These results support the importance of Fe_3O_4 NPs content and PANI and Fe_3O_4 interactions for HER activity of PANI/Fe_3O_4 material. Namely, theoretical considerations by DFT have confirmed that the Gibbs free energy of hydrogen adsorption, as one of the main indicators of material's activity towards catalysis of HER, is reduced in the presence of PANI [47].

Thus, in addition to electrical conductivity, herein observed favourable HER kinetics at PANI/Fe_3O_4-II(3) may be explained by the synergistic effect of PANI and Fe_3O_4 NPs. PANI stabilizes metal/metal oxide NPs [48]. Furthermore, it has been suggested that during HER in acidic media, PANI with abundant electrons on N atoms effectively weakens the bonding of H^+ in H_3O^+ ions and captures H^+, forming protonated amine groups [48]. These H^+ may easily transfer from the protonated amine groups to the surface of metal oxide NPs with a low transfer barrier. Homogeneously distributed Fe_3O_4 NPs of 10 to 50 nm size [19] in PANI/Fe_3O_4-II(3) represent numerous active sites. Finally, the H atoms adsorbed on metal oxide react mutually, generating H_2 gas.

To compare the number of active sites at four PANI/Fe_3O_4 electrocatalysts, their effective surface area (ESA) is evaluated by calculating the double-layer capacitance (C_{dl}). C_{dl} is calculated from cyclic voltammetry plotting the difference $\Delta j = (j_a - j_c)/2$ at 0.1 V *vs.* sweep rate (Figure 3D) [48] and it is found to be 2.4, 1.4, 1.1 and 0.9 μF cm^{-2} for PANI/Fe_3O_4-II(7), PANI/Fe_3O_4-II(3), PANI/Fe_3O_4-I(7) and PANI/Fe_3O_4-I(3), respectively. The obtained C_{dl} value of PANI/Fe_3O_4-II(3) indicates its higher ESA and more active sites for HER compared to PANI/Fe_3O_4-I(3) and PANI/Fe_3O_4-I(7) electrocatalysts.

Furthermore, EPR spectra of PANI/Fe_3O_4 samples previously showed that the intensity of signal originating from Fe_3O_4 NPs decreased with increasing polymerization time for both series of samples (I and II, prepared with mass ratio Fe_3O_4 NPs/aniline of 0.0015 and 0.015, respectively) [19], suggesting that the amount of incorporated Fe_3O_4 NPs relative to the amount of PANI is higher in PANI/Fe_3O_4-II(3) than that in PANI/Fe_3O_4-II(7). This is expected as the PANI yield increases with polymerization time while the total amount of Fe_3O_4 NP catalysts in the reaction system does not change. A higher amount of Fe_3O_4 NPs in PANI/Fe_3O_4-II(3) leads to more pronounced synergistic effects of PANI and Fe_3O_4 NPs toward HER in this sample compared to PANI/Fe_3O_4-II(7). Finally, it should be noted that PANI/Fe_3O_4-II(3) also showed better electrocatalytic performance for HER in comparison with some non-noble metal-based electrocatalysts presented in the literature, Table 2.

Figure 3E shows the polarization curves of PANI/Fe_3O_4-II(3) in 0.1 M H_2SO_4 at a range of temperatures from 25 to 75 °C. Increased cathodic current densities from -23.5 to -60.0 mA cm^{-2} were reached with increasing temperature from 25 to 75 °C. The same behaviour was observed for the rest of the PANI/Fe_3O_4 electrocatalysts. Current density values recorded at different temperatures were used to construct the Arrhenius' regressions, ln *j vs.* T^{-1}, for all electrocatalysts and their slopes were used for the calculation of the apparent activation energy (E_a^{app}) using the Arrhenius equation (Equation 4) [56,57].

$$\frac{\partial \ln|j|}{\partial(1/T)} = \frac{\Delta E_a^{app}}{R} \quad (4)$$

where R is the universal gas constant. The obtained E_a^{app} values increased in the order PANI/Fe_3O_4-II(3) (10 kJ mol^{-1}) < PANI/Fe_3O_4-I(3) (20 kJ mol^{-1}) < PANI/Fe_3O_4-I(7) (23 kJ mol^{-1}) < < PANI/Fe_3O_4-II(7) (39 kJ mol^{-1}). The lowest E_a^{app} of PANI/Fe_3O_4-II(3) correlates well with its best electrocatalytic activity toward HER.

Chronoamperometric curves of four PANI/Fe_3O_4 electrocatalysts are presented in Figure 3F, where a similar current density trend was observed during the polarization study. Namely, PANI/Fe_3O_4-II(3) and PANI/Fe_3O_4-II(7) gave higher current densities during HER than PANI/Fe_3O_4-I(7)

and PANI/Fe_3O_4-I(3). PANI/Fe_3O_4-II(3) showed a current density decrease of *ca.* 21 % during the first 15 min, remaining constant. Some degree of variation in current density with time can originate in the generation of hydrogen gas bubbles at the electrode surface and change in the H^+/H_2 concentration [58]. Moreover, it has been reported that PANI improves stability and reduces current density retention in acidic media by its amino groups capturing H^+, thus keeping it from disrupting the catalyst structure [18].

Activity for HER in electrolytes of a wide pH range could broaden the electrocatalyst's application [23,47]. Hence, the HER performance of PANI/Fe_3O_4-II(3) was also investigated in an 8 M KOH solution as a typical solution used in alkaline industrial water electrolysers, Figure 4A. It could be seen (Figure 4A and 4B) that the activity of PANI/Fe_3O_4-II(3) for HER is notably lower in alkaline than in acidic media as HER onset potential in alkaline media (*ca.* -0.620 V) was found to be *ca.* 330 mV more negative than that in acidic media (-0.289 V). Additionally, the current density reached at -0.5 V in alkaline media (-0.2 mA cm^{-2}) was strikingly lower than in acidic media (-12.0 mA cm^{-2}).

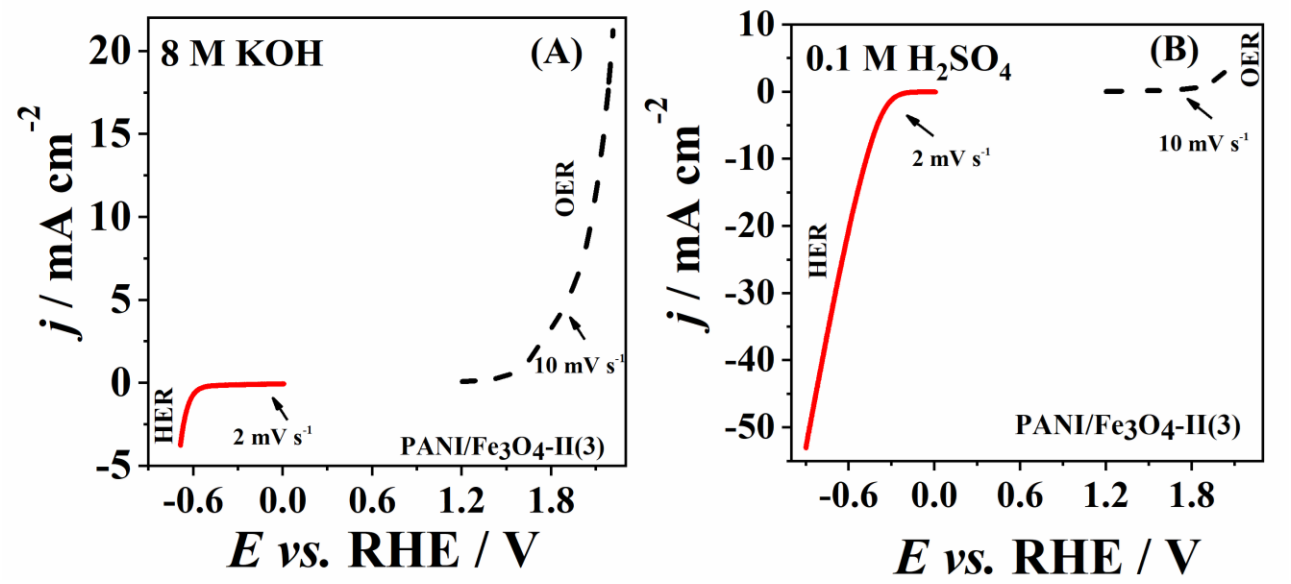

Figure 4. *A: polarization curves of PANI/Fe_3O_4-II(3) electrocatalyst in 8 M KOH for HER and OER; B: polarization curves of PANI/Fe_3O_4-II(3) electrocatalyst in 0.1 M H_2SO_4 for HER and OER*

Furthermore, activity for anode reaction, *i.e.,* oxygen evolution reaction (OER), could broaden the electrocatalyst applicability as a bifunctional electrocatalyst in water electrolysers [59]. Therefore, the OER performance of PANI/Fe_3O_4-II(3) was examined in both acidic (0.1 M H_2SO_4) and alkaline (8 M KOH) media. In the case of OER, higher activity was observed in alkaline than in acidic media in terms of *ca.* 290 mV less positive onset potential (1.60 V in alkaline media *vs.* 1.89 V in acidic media) and *ca.* three times higher current densities reached (7.4 mA cm^{-2} at 2.0 V in alkaline media *vs.* 2.4 mA cm^{-2} in acidic media). Tafel slopes of PANI/Fe_3O_4-II(3) electrocatalyst during OER were determined to be 328 and 289 mV dec^{-1} in alkaline and acidic media, respectively.

Thus, the results obtained in this study suggest that PANI/Fe_3O_4-II(3) is a highly active, low-cost electrocatalyst for HER, which is crucial for efficient, large-scale water-splitting production of hydrogen.

Conclusions

Four PANI/Fe_3O_4 electrocatalysts were tested for HER in acidic media (0.1 M H_2SO_4). The sample PANI/Fe_3O_4-II(3) showed the highest electrocatalytic activity with HER onset potential *ca.* 300 mV

lower than in the case of three other electrocatalysts (-0.286 V *vs.* -0.397, -0.564 and -0.598 V for PANI/Fe_3O_4-II(7), PANI/Fe_3O_4-I(7) and PANI/Fe_3O_4-I(3), respectively) and the highest current density. EIS revealed the lowest charge transfer resistance R_{ct} in the case of PANI/Fe_3O_4-II(3), which, along with its high effective surface area/high content of active sites (as evaluated from C_{dl} value) and the lowest HER activation energy (as calculated from the temperature dependence of current density) could explain its highest HER activity. In addition, the highest content of Fe is measured by EDX for PANI/Fe_3O_4-II(3) sample. Linking PANI and Fe_3O_4 NPs introduced a strong coupling and synergistic effect, a 3D structure with a plethora of exposed active sites, and facile permeation of the electrolyte. Thus, PANI is believed to capture the intermediate H^+ ions and steam their reduction to H_2. The electrocatalytic activity of PANI/Fe_3O_4-II(3) for HER in alkaline media (8 K KOH) as well as for OER in both alkaline and acidic media was explored, offering the possibility of broadening this material's application as bifunctional electrocatalyst in water electrolysers.

Acknowledgements: *The authors would like to thank the Science Fund of the Republic of Serbia, grant number 7750219, Advanced Conducting Polymer-Based Materials for Electrochemical Energy Conversion and Storage, Sensors and Environmental Protection-AdConPolyMat (IDEAS program), as well as the Ministry of Science, Technological Development and Innovation, contracts no. 451-03-65/2024-03/200146 and 451-03-66/2024-03/200146.*

References

[1] L. Huang, Y. Hou, Z. Yu, Z. Peng, L. Wang, J. Huang, B. Zhang, L. Qian, L. Wu, Z. Li, Pt/Fe-NF electrode with high double-layer capacitance for efficient hydrogen evolution reaction in alkaline media, *International Journal of Hydrogen Energy* **42(15)** (2017) 9458-9466. https://doi.org/10.1016/j.ijhydene.2017.02.055

[2] Y. Pan, M. Wen, Noble metals enhanced catalytic activity of anatase TiO_2 for hydrogen evolution reaction, *International Journal of Hydrogen Energy* **43(49)** (2018) 22055-22063. https://doi.org/10.1016/j.ijhydene.2018.10.093

[3] F. Wang, X. Yang, B. Dong, X. Yu, H. Xue, L. Feng, A FeP powder electrocatalyst for the hydrogen evolution reaction, *Electrochemistry Communications* **92** (2018) 33-38. https://doi.org/10.1016/j.elecom.2018.05.020

[4] H. Wang, X. Wang, D. Yang, B. Zheng, Y. Chen, $Co_{0.85}Se$ hollow nanospheres anchored on N-doped graphene nanosheets as highly efficient, nonprecious electrocatalyst for hydrogen evolution reaction in both acid and alkaline media. *Journal of Power Sources* **400** (2018) 232-241. https://doi.org/10.1016/j.jpowsour.2018.08.027

[5] X. Yue, C. Zhong, S. Huang, Y. Jin, C. He, Y. Chen, P.K. Shen, $K_{0.4}TaO_{2.4}F_{0.6}$ Nanocubes as Highly Efficient Noble Metal-Free Electrocatalysts for Hydrogen Evolution Reaction in Acidic Media. *Electrochimica Acta* **245** (2017) 193-200. https://doi.org/10.1016/j.electacta.2017.05.145

[6] J. Deng, P. Ren, D. Deng, L. Yu, F. Yang, X. Bao, Highly active and durable non-precious-metal catalysts encapsulated in carbon nanotubes for hydrogen evolution reaction. *Energy & Environmental Science* **7** (2014) 1919-1923. https://doi.org/10.1039/c4ee00370e

[7] P. Zhang, M. Wang, H. Chen, Y. Liang, J. Sun, L. Sun, A Cu-Based Nanoparticulate Film as Super-Active and Robust Catalyst Surpasses Pt for Electrochemical H_2Production from Neutral and Weak Acidic Aqueous Solutions. *Advanced Energy Materials* **6** (2016) 1502319. https://doi.org/10.1002/aenm.201502319

[8] A.L. Roy, A.M. Shaw, L. Rajagopal, C.H. Strohbehn, S.W. Arendt, K.L. Sauer, Use of minimal-text posters to improve the microbial status of leafy greens and food contact surfaces in foodservice sites serving older adults. *Food Protection Trends* **36** (2016) 125-132. https://doi.org/10.1021/ja403440e

[9] Y. Li, H. Wang, L. Xie, Y. Liang, G. Hong, H. Dai, MoS_2 nanoparticles grown on graphene: An advanced catalyst for the hydrogen evolution reaction, *Journal of the American Chemical Society* **133** (2011) 7296-7299. 7299. https://doi.org/10.1021/ja201269b

[10] M.B. Askari, P. Salarizadeh, M. seifi, S.M. Rozati, A. Beheshti-Marnani, H. Saeidfirozeh, MoCoFeS hybridized with reduced graphene oxide as a new electrocatalyst for hydrogen evolution reaction. *Chemical Physics Letters* **711** (2018) 32-36. https://doi.org/10.1016/j.cplett.2018.09.025

[11] J. Ding, H. Yang, S. Zhang, Q. Liu, H. Cao, J. Luo, X. Liu, Advances in the Electrocatalytic Hydrogen Evolution Reaction by Metal Nanoclusters-based Materials. *Small* **18** (2022) 2204524. https://doi.org/10.1002/smll.202204524

[12] J. Milikić, M. Vasić, L. Amaral, N. Cvjetićanin, D. Jugović, R. Hercigonja, B. Šljukić, NiA and NiX zeolites as bifunctional electrocatalysts for water splitting in alkaline media. *International Journal of Hydrogen Energy* **43** (2018) 18977-18991. https://doi.org/10.1016/j.ijhydene.2018.08.063

[13] Z. Hao, S. Yang, J. Niu, Z. Fang, L. Liu, Q. Dong, S. Song, Y. Zhao, A bimetallic oxide $Fe_{1.89}Mo_{4.11}O_7$ electrocatalyst with highly efficient hydrogen evolution reaction activity in alkaline and acidic media. *Chemical Science* 9 (2018) 5640-5645. https://doi.org/10.1039/c8sc01710g

[14] L. Zhang, Y. Chen, P. Zhao, W. Luo, S. Chen, M. Shao, Fe_3C Nanorods Encapsulated in N-Doped Carbon Nanotubes as Active Electrocatalysts for Hydrogen Evolution Reaction. *Electrocatalysis* **9** (2018) 264-270. https://doi.org/10.1007/s12678-017-0425-3

[15] R. Atchudan, T.N.J. Immanuel Edison, S. Perumal, R. Vinodh, N. Muthuchamy, Y.R. Lee, One-pot synthesis of Fe_3O_4@graphite sheets as electrocatalyst for water electrolysis. *Fuel* **277** (2020) 118235. https://doi.org/10.1016/j.fuel.2020.118235

[16] J. Wang, L. Ji, X. Teng, Y. Liu, L. Guo, Z. Chen, Decoupling half-reactions of electrolytic water splitting by integrating a polyaniline electrode. *Journal of Materials Chemistry A* **7** (2019) 13149-13153. https://doi.org/10.1039/c9ta03285a

[17] M. Wang, L. Jiang, Q. Li, X. Zhou, PANI-modified Pt/$Na_4Ge_9O_{20}$ with low Pt loadings: Efficient bifunctional electrocatalyst for oxygen reduction and hydrogen evolution. *International Journal of Hydrogen Energy* **44** (2019) 31062-31071. https://doi.org/10.1016/j.ijhydene.2019.10.021

[18] G. Ćirić-Marjanović, Recent advances in polyaniline research: Polymerization mechanisms, structural aspects, properties and applications. *Synthetic Metals* **177** (2013) 1-47. https://doi.org/10.1016/j.synthmet.2013.06.004

[19] G. Ćirić-Marjanović. *Polyaniline Nanostructures*, in: A. Eftekhari (Ed.), Nanostructured Conduct. Polym., John Wiley & Sons, Hoboken, New Jersey, 2010: pp. 19-98. https://doi.org/10.1002/9780470661338.ch2

[20] T. Fujisaki, K. Kashima, S. Serrano-Luginbühl, R. Kissner, D. Bajuk-Bogdanović, M. Milojević-Rakić, G. Ćirić-Marjanović, S. Busato, E. Lizundia, P. Walde, Effect of template type on the preparation of the emeraldine salt form of polyaniline (PANI-ES) with horseradish peroxidase isoenzyme C (HRPC) and hydrogen peroxide. *RSC Advances* **9** (2019) 33080-33095. https://doi.org/10.1039/c9ra06168a

[21] M.S. Biserčić, B. Marjanović, B.A. Zasońska, S. Stojadinović, G. Ćirić-Marjanović, Novel microporous composites of MOF-5 and polyaniline with high specific surface area. *Synthetic Metals* **262** (2020) 116348. https://doi.org/10.1016/j.synthmet.2020.116348

[22] D. Wang, L. Yang, H. Liu, D. Cao, Polyaniline-coated Ru/$Ni(OH)_2$ nanosheets for hydrogen evolution reaction over a wide pH range. *Journal of Catalysis* 375 (2019) 249-256. https://doi.org/10.1016/j.jcat.2019.06.008

[23] Z. Duan, K. Deng, C. Li, M. Zhang, Z. Wang, Y. Xu, X. Li, L. Wang, H. Wang, Polyaniline-coated mesoporous Rh films for nonacidic hydrogen evolution reaction. *Chemical Engineering Journal* **428** (2022) 132646. https://doi.org/10.1016/j.cej.2021.132646

[24] B.B. Kamble, S.K. Jha, K.K. Sharma, S.S. Mali, C.K. Hong, S.N. Tayade, Redox active MoO_3-Polyaniline hybrid composite for hydrogen evolution reaction and supercapacitor application. *International Journal of Hydrogen Energy* **48** (2023) 29058-29070. https://doi.org/10.1016/j.ijhydene.2023.04.089

[25] H. Ashassi-Sorkhabi, A. Kazempour, S. Moradi-Alavian, E. Asghari, J.J. Lamb, 3D nanostructured nickel film supported to a conducting polymer as an electrocatalyst with exceptional properties for hydrogen evolution reaction. *International Journal of Hydrogen Energy* **48** (2023) 29865-29876. https://doi.org/10.1016/j.ijhydene.2023.04.139

[26] T.N. Amirabad, A.A. Ensafi, K.Z. Mousaabadi, B. Rezaei, M. Demir, Binder-free engineering design of Ni-MOF ultrathin sheet-like grown on PANI@GO decorated nickel foam as an electrode for in hydrogen evolution reaction and asymmetric supercapacitor. I*nternational Journal of Hydrogen Energy* **48** (2023) 29471-29484. https://doi.org/10.1016/j.ijhydene.2023.04.159

[27] X. Chen, Y. Chen, Z. Shen, C. Song, P. Ji, N. Wang, D. Su, Y. Wang, G. Wang, L. Cui, Self-crosslinkable polyaniline with coordinated stabilized CoOOH nanosheets as a high-efficiency electrocatalyst for oxygen evolution reaction. *Applied Surface Science* **529** (2020) 147173. https://doi.org/10.1016/j.apsusc.2020.147173

[28] Y. Zou, Y. Huang, L.W. Jiang, A. Indra, Y. Wang, H. Liu, J.J. Wang. Polyaniline coating enables electronic structure engineering in Fe_3O_4 to promote alkaline oxygen evolution reaction. *Nanotechnology* **33** (2022) 155402. https://doi.org/10.1088/1361-6528/ac475c

[29] V. Ashok, S. Mathi, M. Sangamithirai, J. Jayabharathi, Regulated Bimetal-Doped Polyaniline: Amorphous-Crumple-Structured Viable Electrocatalyst for an Efficient Oxygen Evolution Reaction. *Energy and Fuels* **36** (2022) 14349-14360. https://doi.org/10.1021/acs.energyfuels.2c03022

[30] Z. Xue, Y. Wang, M. Yang, T. Wang, H. Zhu, Y. Rui, S. Wu, W. An, In-situ construction of electrodeposited polyaniline/nickel-iron oxyhydroxide stabilized on nickel foam for efficient oxygen evolution reaction at high current densities. *International Journal of Hydrogen Energy* **47** (2022) 34025-34035. https://doi.org/10.1016/j.ijhydene.2022.08.023

[31] Y. Duan, Z. Huang, J. Ren, X. Dong, Q. Wu, R. Jia, X. Xu, S. Shi, S. Han, Highly efficient OER catalyst enabled by in situ generated manganese spinel on polyaniline with strong coordination. *Dalton Transactions* **51** (2022) 9116-9126. https://doi.org/10.1039/d2dt01236g

[32] U. Stamenović, N. Gavrilov, I.A. Pašti, M. Otoničar, G. Ćirić-Marjanović, S.D. Škapin, M. Mitrić, V. Vodnik, One-pot synthesis of novel silver-polyaniline-polyvinylpyrrolidone electrocatalysts for efficient oxygen reduction reaction. *Electrochimica Acta* **281** (2018) 549-561. https://doi.org/10.1016/j.electacta.2018.05.202

[33] H. Wang, J. Lin, Z.X. Shen, Polyaniline (PANi) based electrode materials for energy storage and conversion. *Journal of Science: Advanced Materials and Devices* **1** (2016) 225-255. https://doi.org/10.1016/j.jsamd.2016.08.001

[34] C.W. Kuo, J.C. Chang, B.W. Wu, T.Y. Wu, Electrochemical characterization of RuO_2-Ta_2O_5/polyaniline composites as potential redox electrodes for supercapacitors and hydrogen evolution reaction. *International Journal of Hydrogen Energy* **45** (2019) 22223-22231. https://doi.org/10.1016/j.ijhydene.2019.08.059

[35] Y. Chen, Q. Zhang, X. Jing, J. Han, L. Yu, Synthesis of Cu-doped polyaniline nanocomposites (nano Cu@PANI) via the H_2O_2-promoted oxidative polymerization of aniline with copper salt. *Materials Letters* **242** (2019) 170-173. https://doi.org/10.1016/j.matlet.2019.01.143

[36] I. Pašti, M. Milojević-Rakić, K. Junker, D. Bajuk-Bogdanović, P. Walde, G. Ćirić-Marjanović, Superior capacitive properties of polyaniline produced by a one-pot peroxidase/H_2O_2-triggered polymerization of aniline in the presence of AOT vesicles. *Electrochimica Acta* **258** (2017) 834-841. https://doi.org/10.1016/j.electacta.2017.11.133
[37] J. Mišurović, M. Mojović, B. Marjanović, P. Vulić, G. Ćirić-Marjanović, Magnetite nanoparticles-catalysed synthesis of conductive polyaniline. *Synthetic Metals* **257** (2019) 116174. https://doi.org/10.1016/j.synthmet.2019.116174
[38] J. Stejskal, R.G. Gilbert, Polyaniline. Preparation of a conducting polymer(IUPAC Technical Report), *Pure and Applied Chemistry* **74** (2002) 857-867. https://doi.org/10.1351/pac200274050857
[39] E.T. Kang, K.G. Neoh, K.L. Tan, Polyaniline: A polymer with many interesting intrinsic redox states. *Progress in Polymer Science* **23** (1998) 277-324. https://doi.org/10.1016/S0079-6700(97)00030-0
[40] P. Ahuja, S.K. Ujjain, I. Arora, M. Samim, Hierarchically Grown NiO-Decorated Polyaniline-Reduced Graphene Oxide Composite for Ultrafast Sunlight-Driven Photocatalysis. *ACS Omega Journal* **3** (2018) 7846-7855. https://doi.org/10.1021/acsomega.8b00765
[41] S. Golczak, A. Kanciurzewska, M. Fahlman, K. Langer, J.J. Langer, Comparative XPS surface study of polyaniline thin films. *Solid State Ionics* **179** (2008) 2234-2239. https://doi.org/10.1016/j.ssi.2008.08.004
[42] H. Peng, G. Ma, K. Sun, J. Mu, X. Zhou, Z. Lei, A novel fabrication of nitrogen-containing carbon nanospheres with high rate capability as electrode materials for supercapacitors. *RSC Advances* **5** (2015) 12034-12042. https://doi.org/10.1039/c4ra11889h
[43] S. Cho, O.S. Kwon, S.A. You, J. Jang, Shape-controlled polyaniline chemiresistors for high-performance DMMP sensors: Effect of morphologies and charge-transport properties. *Journal of Materials Chemistry* ***A*** **1** (2013) 5679-5688. https://doi.org/10.1039/c3ta01427d
[44] H.A. Bandal, A.R. Jadhav, A.H. Tamboli, H. Kim, Bimetallic iron cobalt oxide self-supported on Ni-Foam: An efficient bifunctional electrocatalyst for oxygen and hydrogen evolution reaction. *Electrochimica Acta* **249** (2017) 253-262. https://doi.org/10.1016/j.electacta.2017.07.178
[45] A.P. Murthy, J. Theerthagiri, J. Madhavan, K. Murugan, Highly active MoS_2/carbon electrocatalysts for the hydrogen evolution reaction - Insight into the effect of the internal resistance and roughness factor on the Tafel slope. *Physical Chemistry Chemical Physics* **19** (2017) 1988-1998. https://doi.org/10.1039/C6CP07416B
[46] N. Lingappan, I. Jeon, W. Lee, Polyaniline induced multi-functionalities in interfacially coupled electrocatalysts for hydrogen/oxygen evolution reactions. *Journal of Materials Chemistry A* **11** (2023) 17797-17809. https://doi.org/10.1039/d3ta02389c
[47] F. Meng, Y. Yu, D. Sun, S. Lin, X. Zhang, T. Xi, C. Xu, H. Ouyang, W. Chu, L. Shang, Q. Su, B. Xu, Three-Dimensional Needle Branch-like PANI/CoNiP Hybrid Electrocatalysts for Hydrogen Evolution Reaction in Acid Media. *ACS Applied Energy Materials Journal* **4** (2021) 2471-2480. https://doi.org/10.1021/acsaem.0c03033
[48] Q. Dang, Y. Sun, X. Wang, W. Zhu, Y. Chen, F. Liao, H. Huang, M. Shao, Carbon dots-Pt modified polyaniline nanosheet grown on carbon cloth as stable and high-efficient electrocatalyst for hydrogen evolution in pH-universal electrolyte. *ACS Applied Energy Materials Journal* **257** (2019) 117905. https://doi.org/10.1016/j.apcatb.2019.117905
[49] C.C.L.L. McCrory, S. Jung, I.M. Ferrer, S.M. Chatman, J.C. Peters, T.F. Jaramillo, Benchmarking Hydrogen Evolving Reaction and Oxygen Evolving Reaction Electrocatalysts for Solar Water Splitting Devices. *Journal of the American Chemical Society* **137** (2015) 4347-4357. https://doi.org/10.1021/ja510442p

[50] P. Yu, L. Wang, Y. Xie, C. Tian, F. Sun, J. Ma, M. Tong, W. Zhou, J. Li, H. Fu, High-Efficient, Stable Electrocatalytic Hydrogen Evolution in Acid Media by Amorphous Fe_xP Coating Fe_2N Supported on Reduced Graphene Oxide. *Small* **14** (2018) 1801717. https://doi.org/10.1002/smll.201801717

[51] B. Konkena, K.J. Puring, I. Sinev, S. Piontek, O. Khavryuchenko, J.P. Dürholt, R. Schmid, H. Tüysüz, M. Muhler, W. Schuhmann, U.P. Apfel, Pentlandite rocks as sustainable and stable efficient electrocatalysts for hydrogen generation. *Nature Communications* **7** (2016) 12269. https://doi.org/10.1038/ncomms12269

[52] Y. Ge, P. Dong, S.R. Craig, P.M. Ajayan, M. Ye, J. Shen, Transforming Nickel Hydroxide into 3D Prussian Blue Analogue Array to Obtain Ni_2P/Fe_2P for Efficient Hydrogen Evolution Reaction, A*dvanced Energy Materials* 8 (2018) 1800484. https://doi.org/10.1002/aenm.201800484

[53] T.H. Wondimu, G.C. Chen, D.M. Kabtamu, H.Y. Chen, A.W. Bayeh, H.C. Huang, C.H. Wang, Highly efficient and durable phosphine reduced iron-doped tungsten oxide/reduced graphene oxide nanocomposites for the hydrogen evolution reaction. *International Journal of Hydrogen Energy* **43** (2018) 6481-6490. https://doi.org/10.1016/j.ijhydene.2018.02.080

[54] L. Tian, X. Yan, X. Chen. Electrochemical Activity of Iron Phosphide Nanoparticles in Hydrogen Evolution Reaction. *ACS Catalysis Journal* **6** (2016) 5441-5448. https://doi.org/10.1021/acscatal.6b01515

[55] D.A. Dalla Corte, C. Torres, P.D.S. Correa, E.S. Rieder, C.D.F. Malfatti. The hydrogen evolution reaction on nickel-polyaniline composite electrodes. *International Journal of Hydrogen Energy* **37** (2012) 3025-3032. https://doi.org/10.1016/j.ijhydene.2011.11.037

[56] J. Milikić, G. Ćirić-Marjanović, S. Mentus, D.M.F. Santos, C.A.C. Sequeira, B. Šljukić, Pd/c-PANI electrocatalysts for direct borohydride fuel cells. *Electrochimica Acta* **213** (2016) 298-305. https://doi.org/10.1016/j.electacta.2016.07.109

[57] A.J. Bard, L.R. Faulkner, *Electrochemical Methods: Fundamentals and Applications*, 2nd ed., John Wiley & Sons, New York, United States, 2001, p. 864. ISBN 978-0471043720

[58] B. Kurt Urhan, H. Öztürk Doğan, T. Öznülüer Özer, Ü. Demir, Palladium-coated polyaniline nanofiber electrode as an efficient electrocatalyst for hydrogen evolution reaction. *International Journal of Hydrogen Energy* **47** (2022) 4631-4640. https://doi.org/10.1016/j.ijhydene.2021.11.101

[59] C. Feng, M.B. Faheem, J. Fu, Y. Xiao, C. Li, Y. Li, Fe-Based Electrocatalysts for Oxygen Evolution Reaction: Progress and Perspectives. *ACS Catalysis Journal* **10** (2020) 4019-4047. https://doi.org/10.1021/acscatal.9b05445